

# Photophysical Aspects of Single-Molecule Detection by Two-Photon Excitation with Consideration of Sequential Pulsed Illumination

R. Niesner, W. Roth, and Karl-Heinz Gericke\*<sup>[a]</sup>

*An important goal in single molecule fluorescence correlation spectroscopy is the theoretical simulation of the fluorescence signal stemming from individual molecules and its autocorrelation function. The simulation approaches developed up to now are based exclusively on continuous-wave (cw) illumination and consequently on cw-excitation. However, this approximation is no longer valid in the case of two-photon excitation, for which pulsed illumination is usually employed. We present a novel theoretical model for the simulation of the fluorescence signal of single molecules and its autocorrelation function with consideration of the time dependence of the excitation flux and thus of all illumination-dependent photoprocesses: two-photon excitation, induced emission and photobleaching. Further important characteristics of our approach are the consideration of the dependence*

*of the photobleaching rate on illumination and the low intersystem-crossing rates of the studied coumarins. Moreover, using our approach, we can predict quantitatively the effect of the laser pulse width on the fluorescence signal of a molecule, that is, the contributions of the photobleaching and saturation effects, and thus we can calculate the optimal laser pulse width. The theoretical autocorrelation functions were fitted to the experimental data, and we could ascertain a good agreement between the resulting and the expected parameters. The most important parameter is the photobleaching constant  $\sigma$ , the cross section of the transition  $S_n \leftarrow S_1$ , which characterises the photostability of the molecules independent of the experimental conditions. Its value is  $1.7 \times 10^{-23} \text{ cm}^2$  for coumarin 153 and  $5 \times 10^{-23} \text{ cm}^2$  for coumarin 314.*

## 1. Introduction

The detection of individual fluorescent molecules by laser-induced fluorescence microscopy opened new horizons for the investigation of dynamics in such heterogeneous systems as are met in analytical chemistry, biology and medicine.<sup>[1–3]</sup> In this respect, fluorescence correlation spectroscopy (FCS) has proved to be a powerful tool for analysis of molecular dynamics and photodynamics at room temperature by one- and two-photon excitation.<sup>[1,2,4,5]</sup> An important step in the evolution of FCS is the development of suitable theoretical models for the simulation of the fluorescence autocorrelation functions.

One of the first models (Aragon and Pecora), which considers translational and rotational diffusion and chemical reactions, is based on a modified first law of diffusion and generally describes the autocorrelation functions obtained by FCS.<sup>[5–7]</sup> From the time profile of the autocorrelation functions thus obtained local diffusion coefficients and rates of different chemical reactions can be determined.<sup>[5,8]</sup> Application of this model has also been extended to single-molecule FCS.

However, not only transport processes and chemical reactions but also photophysical processes affect the fluorescence signal and its autocorrelation function. Thus, new theoretical models had to be developed to obtain the kinetic rates of these photophysical processes, for example, intersystem crossing (ISC).<sup>[9,10]</sup> The model, which includes triplet-state dynamics, is derived from the approach of Aragon and Pecora and describes the behaviour of the molecule in the excitation volume with a closed three-level approach, that is, the molecule can reside only in the states  $S_0$ ,  $S_1$  or  $T_1$ .

An undesired process which limits the number of fluorescence photons emitted by an individual molecule and thus strongly affects the features of the autocorrelation function is photobleaching, defined as the irreversible photophysical interruption of the excitation–emission cycles between  $S_0$  and  $S_1$ . Thus, determination of the photobleaching parameters is crucial for selecting appropriate dyes for single-molecule FCS experiments. The difficulties in rigorously describing the process of photobleaching arise from the multitude of photobleaching mechanisms which must be considered in a theoretical approach. Some groups have developed models which take into account different photobleaching mechanisms, for example, illumination-independent photobleaching by the singlet and triplet states and illumination-dependent photobleaching by two-step photolysis.<sup>[11–14]</sup> The derived mathematical expression for the simulated autocorrelation function has largely been employed for approximating autocorrelation curves achieved by one-photon excitation (OPE) and two-photon excitation (TPE).<sup>[15,16]</sup> An important insight thus attained is that a major contribution to the process of photobleaching results from photobleaching via triplet states.<sup>[14]</sup> Note that all these models are designed for the case of either one- or two-photon cw ex-

[a] R. Niesner, Dr. W. Roth, Prof. Dr. K.-H. Gericke  
Institut für Physikalische und Theoretische Chemie  
Technische Universität Braunschweig  
Hans-Sommer-Str. 10, 38106 Braunschweig  
Fax: (+49) 531-391-5396  
E-mail: k.gericke@tu-braunschweig.de

citation. However, in two-photon excitation experiments pulsed illumination is usually employed, and, as was already pointed out by Mertz, this kind of illumination has severe consequences for the multiphoton excitation rate as compared to cw illumination.<sup>[17]</sup> Mertz defines in his model a set of differential equations which describes the occurring photophysical processes (excitation, induced emission, photobleaching, fluorescence and intersystem crossing) with consideration of pulsed multiphoton excitation. Combining this set of equations with a modified second law of diffusion leads to the autocorrelation function of the fluorescence signal of a molecule under pulsed illumination. In this framework, the photobleaching parameter (quantum yield of photobleaching) is assumed to be a constant that is independent of the pulsed excitation flux.<sup>[17]</sup> However, in the following discussion the comparison of simulated with experimental data shows that the photobleaching yield depends strongly on the excitation flux and is thus a time-dependent parameter.<sup>[17]</sup> Nevertheless, the model was not subsequently corrected for a time-dependent photobleaching parameter.

We developed a kinetic rate model to simulate the fluorescence autocorrelation functions obtained by two-photon excitation. The main novel feature of our model is that it considers the effect of pulsed illumination on all intensity-dependent photoprocesses, that is, not only two-photon excitation but also photobleaching and induced emission. Whereas all former cw models consider steady state conditions, we perform a time-dependent treatment, which is essential for all pulsed photoprocesses.

Experiments were performed with coumarin 153 (C153) and coumarin 314 (C314). Therefore, our model considers the special case of these dyes, which are characterised by low rates of ISC<sup>[18–20]</sup> relative to other coumarins and rhodamines.<sup>[14]</sup> Consequently, all photoprocesses involving triplet states proceed very slowly compared to fluorescence and can be neglected. Thus, photobleaching through the major channel, that is, higher triplet states, does not occur. The only possible loss channel is photobleaching through singlet states. As far as the photobleaching rate (the rate of the transition  $S_n \leftarrow S_1$ ) is concerned, we assume that it scales linearly with the excitation flux  $\phi$  and consequently that the ground state depletion rate scales with the third power of the excitation flux. This assumption is in good agreement both with our experimental results and with the results of other authors obtained when ignoring ISC.<sup>[16,17,21]</sup> In other words, the molecule undergoes photobleaching if it reaches  $S_n$ , from which it cannot return to the ground state  $S_0$ . The relevant transitions are presented in Figure 1.

Since the photobleaching rate depends on the excitation flux, which in turn is described by a time function given by the characteristics of the laser, photobleaching is switched on during the laser pulse and switched off after it. Thus, photobleaching is a time-dependent process like excitation and induced emission.

Evident proof that consideration of time-dependent excitation flux is necessary is provided by comparing the photobleaching rates obtained with the well-known cw model and

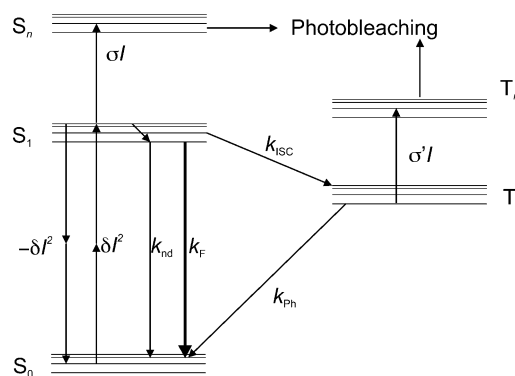


**Figure 1.** Simplified Jablonski diagram. Molecular constants:  $\delta$  = two-photon excitation cross section,  $\sigma$  = cross section of the transition  $S_n \leftarrow S_1$  (photobleaching constant),  $\sigma'$  = cross section of the transition  $T_n \leftarrow T_1$  (photobleaching constant). Transition rates:  $k_{nd}$  = rate of nonradiative decay  $S_0 \leftarrow S_1$ ,  $k_f$  = fluorescence rate,  $k_{ph}$  = phosphorescence rate,  $k_{ISC}$  = intersystem crossing rate,  $\delta\phi^2$  = two-photon excitation rate,  $-\delta\phi^2$  = rate of induced emission,  $\sigma\phi$  = rate of the transition  $S_n \leftarrow S_1$ ,  $\sigma'\phi$  = rate of the transition  $T_n \leftarrow T_1$ . The relaxation rate  $k$  is defined as  $k = k_{nd} + k_f$  and can be calculated as  $k = 1/\tau_p$  where  $\tau_p$  is the fluorescence lifetime. The fluorescence rate  $k_f$  can be determined as  $k_f = \phi_f/\tau_p$  where  $\phi_f$  is the fluorescence quantum yield.

our model. The former are up to six orders of magnitude larger than the latter.

We measured the molecular specific cross section  $\sigma$  of the transition  $S_n \leftarrow S_1$ , which characterises the photobleaching process. Using this constant we can compare the photostability of substances with low ISC rates independent of the excitation flux at which it was determined. Usually, the photostability of substances is compared in terms of ground-state depletion rate or photobleaching yield.<sup>[14]</sup> However, these indicators depend, for example, on the excitation flux (laser power), and therefore they are specific and different for each experiment.

## 2. Kinetic Rate Model

The fluorescence signal of a molecule is directly proportional to the population of the first excited state. Thus, to obtain the most probable time profile of the fluorescence signal  $F(t)$  of an individual molecule, the probability of occupancy of the first singlet state  $S_1(t)$  must be determined. By employing a kinetic rate model which includes photophysical processes and diffusion, the time dependence of the probability of occupancy of  $S_1$  can be obtained.

Since we are interested in the photophysical behaviour of C153 and C314 molecules and these undergo practically no ISC, we will consider in our model only irreversible photobleaching through higher singlet states via  $S_n \leftarrow S_1$  transitions. Phosphorescence and photobleaching through triplet states can be neglected in this case. Furthermore, we assume that the rate of nonradiative conversion in  $S_1$  is sufficiently large that, after the pulse, the molecule has a high probability of being in the vibrational ground state of  $S_1$ . Consequently, the photobleaching rate is considered to scale linearly with the excitation flux. An approximation of the photobleaching rate by a constant results in FCS functions which are not validated by

our experimental data: the resulting photobleaching rates are not constant for different laser powers but scale linearly with the excitation flux. This is unequivocal evidence that the rate of ground-state depletion scales cubically with the excitation flux.

We consider an individual molecule which repeatedly undergoes two-photon excitation and emission as it freely diffuses through a defined volume  $V$ , the effective excitation volume. The absorption–fluorescence cycles are interrupted by diffusion out of the volume  $V$  or by photobleaching.

The effective TPE volume  $V$  is defined in Equation (1)<sup>[22]</sup>

$$V = \frac{\int \int h^2(r, z) 2\pi r dr dz}{\int \int h^4(r, z) 2\pi r dr dz} = \gamma^{-1} \int \int h^2(r, z) 2\pi r dr dz \quad (1)$$

where  $r$  and  $z$  are cylindrical coordinates,  $\gamma$  is the volume contrast and  $h(r, z)$  the point spread function, that is, the unitless intensity profile.<sup>[22]</sup> For the evaluation of  $V$  we approximate the point spread function  $h(r, z)$  by a 2D-Gaussian–Lorentzian distribution.<sup>[22]</sup> The expansions of the volume  $V$  are the principal  $1/e^2$  limited axis  $z_e$  on the optical axis and the secondary  $1/e^2$  limited axis  $\omega_0$  in the focal plane.

The diffusion of the molecule through the excitation volume is quantified by the mean diffusion time  $\tau_D$  calculated for a 2D-Gaussian–Lorentzian intensity profile [Eq. (2)]<sup>[17]</sup>

$$\tau_D = \frac{\omega_0^2}{1.8D} \ln\left(\frac{6z_e}{\omega_0}\right) \quad (2)$$

where  $D$  is the local diffusion coefficient. Since the excitation volume is much smaller than the sample volume, the photobleached molecules can be replaced by new molecules diffusing into the excitation volume, so that competition between diffusion and photobleaching occurs. The renewal of the bleached molecules is taken into consideration by defining the diffusion time as the mean diffusion time according to Mertz, that is, the period between the molecule's first entering the excitation volume and leaving it for the last time.<sup>[17]</sup>

As mentioned in the introduction, an important difference between one- and two-photon fluorescence microscopy is that in the former cw, and in the latter pulsed illumination, is usually employed. The effects of pulsed as opposed to cw illumination have significant consequences for the photobleaching rate, the excitation rate and the rate of induced emission. Thus, it is important to regard the excitation flux in our model as a time function  $\phi(r, z, t')$  which restores the time profile of the laser pulses ( $t'$  represents the time axis during the period including the laser pulse and the dark period thereafter). The excitation flux is the time-dependent excitation intensity at the sample with units of photon  $\text{cm}^{-2} \text{s}^{-1}$ .

To simplify our approach, we introduce two approximations concerning the excitation flux  $\phi(r, z, t')$ :

- 1) The excitation volume is uniformly illuminated, that is, the point spread function  $h(r, z)$  is constant within the limits  $\omega_0$  and  $z_e$ , and zero outside.
- 2) The time profile of the laser pulse is rectangular.

The first simplification is justified as long as the excitation volume  $V$  is small (holds for TPE). The second approximation does not significantly influence the time profile of the fluorescence signal and its autocorrelation function.<sup>[17]</sup> Mathematically, the simplified excitation flux can be expressed as Equations (3) and (4)

$$\phi(r, z, t') = \frac{I(t')}{\pi\omega_0^2} \quad (3)$$

$$I(t') = \begin{cases} I_0, & t' \in [0, \tau_p] \\ 0, & t' \in [\tau_p, \tau_0] \end{cases} \quad (4)$$

where  $\tau_p$  is the pulse width,  $1/\tau_0$  is the repetition rate of the laser and  $I_0$  is the peak intensity at the geometric focal centre. In the following, we denote the function  $\phi(r, z, t')$  as  $\phi(t')$  and the peak flux  $I_0(\pi\omega_0^2)^{-1}$  as  $\phi_0$ .

Under these assumptions, the set of differential equations describing the behaviour of an individual C153 or C314 molecule inside the excitation volume  $V$  according to Figure 1 is given by Equation (5).

$$\frac{d}{dt'} \begin{pmatrix} S_0(t') \\ S_1(t') \end{pmatrix} = \begin{pmatrix} -\delta\phi^2(t') - \frac{1}{\tau_D} & \delta\phi^2(t') + k \\ \delta\phi^2(t') & -\delta\phi^2(t') - k_F - \sigma\phi(t') - \frac{1}{\tau_D} \end{pmatrix} \begin{pmatrix} S_0(t') \\ S_1(t') \end{pmatrix}. \quad (5)$$

Thereby, we took into consideration that the populations of the  $S_0$  and  $S_1$  states can be reduced by both photophysical processes and diffusion.

To solve this set of equations, we employed an iterative method based on the following physical insights:

- 1) During the laser pulse the molecule practically does not relax in  $S_0$  (fluorescence or nonradiative decay;  $\tau_F \gg \tau_p$ ;  $\tau_F$  is typically of the order of a few nanoseconds, while  $\tau_p$  is on the femtosecond timescale) and has insufficient time to diffuse out of the excitation volume ( $\tau_D \gg \tau_p$ ;  $\tau_D$  is on the order of micro- or milliseconds).
- 2) After the laser pulse, the molecule relaxes in  $S_0$  (fluorescence or nonradiative decay) and can diffuse out of the observation volume, but it can be neither excited nor photobleached ( $\delta\phi^2(t') = 0$ ,  $\sigma\phi(t') = 0$ ).

Hence, we can divide the former set of differential equations [Eq. (5)] into one set considering the period during the pulse  $[0, \tau_p]$  [Eq. (6)] and another considering the "dark period"  $\tau_0$  after the pulse  $[\tau_p, \tau_0]$  [Eq. (9)].

During a laser pulse  $i$ , the molecule can absorb two photons, can undergo induced emission and can be photobleached. Thus, the set of differential equations describing the behaviour of the molecule during the pulse is Equation (6)

$$\frac{d}{dt'} \begin{pmatrix} S_{0p}^i(t') \\ S_{1p}^i(t') \end{pmatrix} = \begin{pmatrix} -\delta\phi_0^2 & \delta\phi_0^2 \\ \delta\phi_0^2 & -\delta\phi_0^2 - \sigma\phi_0 \end{pmatrix} \begin{pmatrix} S_{0p}^i(t') \\ S_{1p}^i(t') \end{pmatrix} \quad (6)$$

with the initial conditions of Equation (7).

$$\begin{pmatrix} S_{0p}^i(0) \\ S_{1p}^i(0) \end{pmatrix} = \begin{pmatrix} a^i \\ b^i \end{pmatrix} \quad (7)$$

The additional index "p" for  $S_0(t)$  and  $S_1(t)$  denotes that these functions are calculated for  $t$  in  $[0, \tau_p]$ .

The solution of Equation (6) is given by Equation (8).

$$\begin{pmatrix} S_{0p}^i(t') \\ S_{1p}^i(t') \end{pmatrix} = \begin{pmatrix} g_1(t') & g_2(t') \\ g_2(t') & g_3(t') \end{pmatrix} \begin{pmatrix} a^i \\ b^i \end{pmatrix} \quad (8)$$

The functions  $g_1(t')$ ,  $g_2(t')$  and  $g_3(t')$  depend on the TPE cross section  $\delta$ , the excitation flux  $\phi_0$  and the cross section  $\sigma$  of the transition  $S_n \leftarrow S_1$ .

The second set of equations describing the transport and photoprocesses during the period  $\tau_0$  between two consecutive laser pulses, that is, the dark period, is Equation (9):

$$\frac{d}{dt'} \begin{pmatrix} S_{0d}^i(t') \\ S_{1d}^i(t') \end{pmatrix} = \begin{pmatrix} -\frac{1}{\tau_D} & k \\ 0 & -k - \frac{1}{\tau_D} \end{pmatrix} \begin{pmatrix} S_{0d}^i(t') \\ S_{1d}^i(t') \end{pmatrix} \quad (9)$$

with the initial conditions of Equation (10)].

$$\begin{pmatrix} S_{0d}^i(\tau_p) \\ S_{1d}^i(\tau_p) \end{pmatrix} = \begin{pmatrix} c^i \\ d^i \end{pmatrix} \quad (10)$$

The additional index  $d$  for  $S_0(t)$  and  $S_1(t)$  denotes that these functions are calculated during the dark period between two consecutive laser pulses.

By solving the set of differential equations (9), we obtain Equation (11)

$$\begin{pmatrix} S_{0d}^i(t') \\ S_{1d}^i(t') \end{pmatrix} = \begin{pmatrix} g_4(t') & g_5(t') \\ 0 & g_6(t') \end{pmatrix} \begin{pmatrix} c^i \\ d^i \end{pmatrix} \quad (11)$$

<sup>1</sup> The expressions of the functions  $g_1(t')$ ,  $g_2(t')$  and  $g_3(t')$  used for the calculation of the probability of occupancy of the first singlet state  $S_1$  immediately after the laser pulse are given by Equations (a)–(d)

$$\Sigma = \sqrt{4\delta^2\phi_0^2 + \sigma^2} \quad (a)$$

$$g_1(t') = \frac{e^{-\frac{1}{2}\phi_0 t' (2\phi_0\delta + \sigma + \Sigma)}}{2\Sigma} [(-1 + e^{\phi_0 t' \Sigma})\sigma + (1 + e^{\phi_0 t' \Sigma})\Sigma] \quad (b)$$

$$g_2(t') = \frac{e^{-\frac{1}{2}\phi_0 t' (2\phi_0\delta + \sigma + \Sigma)} (-1 + e^{\phi_0 t' \Sigma}) \phi_0 \delta}{\Sigma} \quad (c)$$

$$g_3(t') = \frac{e^{-\frac{1}{2}\phi_0 t' (2\phi_0\delta + \sigma + \Sigma)}}{2\Sigma} [(1 - e^{\phi_0 t' \Sigma})\sigma + (1 + e^{\phi_0 t' \Sigma})\Sigma] \quad (d)$$

<sup>2</sup> The expressions of the functions  $g_4(t')$ ,  $g_5(t')$  and  $g_6(t')$  used for calculating the probability of occupancy of the first singlet state  $S_1$  after the dark period are given by Equations (e)–(g).

$$g_4(t') = e^{-t'/\tau_D} \quad (e)$$

$$g_5(t') = (e^{kt} - 1)g_6(t') \quad (f)$$

$$g_6(t') = e^{-(k+1/\tau_D)t} \quad (g)$$

where the functions  $g_4(t')$ ,  $g_5(t')$  and  $g_6(t')$  depend on the mean diffusion time  $\tau_D$  and on the relaxation rate  $k$ .<sup>2</sup>

Since the total excitation is characterised by a periodical "train" of laser pulses, the populations of the ground state  $S_0$  and of the first singlet state  $S_1$  are also oscillations. However, the oscillations of  $S_0(t')$  and  $S_1(t')$  are not purely periodical, but are damped due to photobleaching and diffusion. These processes remove the molecule from the excitation–emission cycle between  $S_0$  and  $S_1$ . Consequently, the initial conditions  $a^i, b^i$  at the laser pulse  $i$  are the results of the diffusion–fluorescence set of Equations (9) of the foregoing dark period  $i-1$  at time  $t' = \tau_0$ . The initial conditions  $c^i, d^i$  in the dark period  $i$  are the results of the excitation–photobleaching set of equations (6) of the same pulse  $i$  at time  $t' = \tau_p$ . The initial conditions  $a^i, b^i, c^i, d^i$  resulting from sets of Equations (6) and (9) are given by Equation (12).

$$\begin{pmatrix} a^i \\ b^i \end{pmatrix} = \begin{pmatrix} S_{0d}^{i-1}(\tau_0) \\ S_{1d}^{i-1}(\tau_0) \end{pmatrix} \quad \text{and} \quad \begin{pmatrix} c^i \\ d^i \end{pmatrix} = \begin{pmatrix} S_{0p}^i(\tau_p) \\ S_{1p}^i(\tau_p) \end{pmatrix} \quad (12)$$

Since we observe the fluorescence signal of an individual molecule integrated over the dark interval  $[\tau_p, \tau_0]$  [Eq. (13)]

$$F^i = S_{1p}^i(\tau_p) \int_{\tau_p}^{\tau_0} k_F e^{-t'/\tau_F} dt' = S_{1p}^i(\tau_p) f_0 \quad (13)$$

we must determine only  $S_{1p}^i(\tau_p) = d^i$  to obtain the dependence of the fluorescence signal on the pulse position, because  $f_0$ , the integral in Equation (13), is independent of  $i$ .

Considering expressions (12), which connect the results attained during two successive cycles containing a laser pulse and the dark period thereafter, we obtain Equation (14).

$$\begin{pmatrix} c^i \\ d^i \end{pmatrix} = \begin{pmatrix} g_1(\tau_p) & g_2(\tau_p) \\ g_2(\tau_p) & g_3(\tau_p) \end{pmatrix} \begin{pmatrix} g_4(\tau_0) & g_5(\tau_0) \\ 0 & g_6(\tau_0) \end{pmatrix} \begin{pmatrix} c^{i-1} \\ d^{i-1} \end{pmatrix} \quad (14)$$

The index  $i=1$  is assigned to the reference pulse which first interacts with the molecule as it enters the volume  $V$ . Moreover, we consider that the molecule is necessarily in the ground state as it diffuses into volume  $V$ . Thus, the initial conditions of set (6) for  $i=1$  is given by Equation (15)]:

$$\begin{pmatrix} a^1 \\ b^1 \end{pmatrix} = \begin{pmatrix} 1 \\ 0 \end{pmatrix} \quad (15)$$

Applying Equation (15) to Equation (14), we obtain Equation (16):

$$\begin{pmatrix} c^i \\ d^i \end{pmatrix} = \begin{pmatrix} g_1(\tau_p) & g_2(\tau_p) \\ g_2(\tau_p) & g_3(\tau_p) \end{pmatrix} \left[ \begin{pmatrix} g_4(\tau_0) & g_5(\tau_0) \\ 0 & g_6(\tau_0) \end{pmatrix} \begin{pmatrix} g_1(\tau_p) & g_2(\tau_p) \\ g_2(\tau_p) & g_3(\tau_p) \end{pmatrix} \right]^{i-1} \begin{pmatrix} 1 \\ 0 \end{pmatrix} \quad (16)$$

which gives the probability of occupancy of  $S_0$  and  $S_1$  for each pulse  $i$  at the beginning of the dark period.

Since we can consider that the period  $\tau_0$  signifies a time unit, the index  $i$  is a time dimension and can be expressed by Equation (17).

$$i = \frac{t}{\tau_0} \quad (17)$$

Thus, we can write  $c^i = c(t)$  and  $d^i = d(t)$ , where  $t$  is the time variable with unit  $\tau_0$ . The probability of occupancy of the first singlet state at the end of the laser pulse is  $S_{1p}(t; \tau_p) = d(t)$ . Consequently, the most probable time profile of the fluorescence signal of an individual molecule is given by Equation (18).

$$F(t) = S_{1p}(t; \tau_p) f_0 \quad (18)$$

Note that the fluorescence signal  $F(t)$  of a single molecule is not equivalent to the fluctuating fluorescence signal registered in the experiment, since during data acquisition many molecules are monitored. Nevertheless, the molecules are detected one at a time. The signal  $F(t)$  restores only the most probable time profile of the experimental fluorescence bursts emitted by single molecules when the background is neglected, that is,  $F(t)$  is an averaged fluorescence signal over a very large number of molecules and thus a statistical quantity.

Since the autocorrelation analysis used in the evaluation of the experimental signal is an integrative method, through which the properties of the individual burst are lost and only the average characteristics of the fluctuations are retained, the assumption that the experimental autocorrelation functions and the autocorrelation functions of the simulated signal  $F(t)$  are equivalent is justified. The theoretical autocorrelation function is defined by Equation (19).

$$G(\tau) = \frac{\langle \delta F(t) \delta F(t + \tau) \rangle}{\langle \delta F(t) \rangle^2} \quad (19)$$

where  $\delta F(t) = F(t) - \langle F(t) \rangle$ .

However, this function  $G(\tau)$  is defined for the special case of an average number  $N$  of one molecule in the excitation volume ( $N=1$ ) without taking into account the background. When considering the background and an arbitrary  $N$ , the simulated autocorrelation function becomes Equation (20)

$$G_{\text{fit}}(\tau) = G(0_+) G(\tau) \quad (20)$$

where  $G(0_+)$  is the amplitude of the autocorrelation function without considering the photobleaching defined in Equation (21)<sup>[22]</sup>

$$G(0_+) = \frac{\xi^2}{N} = \frac{[I_F / (I_F + I_B)]^2}{N} \quad (21)$$

where  $I_F$  is the mean fluorescence signal, and  $I_B$  the mean background signal.<sup>[22, 23]</sup> The term which restores the influence of photobleaching on the amplitude of the autocorrelation functions is included in the function  $G(\tau)$ .

By fitting  $G_{\text{fit}}(\tau)$  to the experimental autocorrelation functions, the diffusion time  $\tau_D$ , the photobleaching cross section  $\sigma$  and the average number of molecules in the excitation volume  $N$  can be determined.

### 3. Experiment

The basic setup used to register the fluorescence signal in single-molecule experiments is similar to that described by Mertz et al.,<sup>[22]</sup> with the following differences: the laser beam is tenfold extended, and the repetition rate of the Ti:Sa laser (Mira 900, Coherent) is not doubled. The pulsed laser beam has 200 fs pulse width and 76 MHz repetition rate. The pulse width at the sample is approximately 300 fs,<sup>[24]</sup> broadened from 200 fs by group delay dispersion mainly in the objective (BK7).<sup>[25]</sup> A microscope objective Plan Neofluar (40 $\times$ , NA=1.3, oil-immersion, Carl Zeiss) is used to focus the extended laser beam in the sample. The dimensions of the effective two-photon excitation volume calculated as indicated in Section 2 are  $\omega_0 = 334$  nm,  $z_e = 1570$  nm and  $V \approx 0.74$  fL for an excitation wavelength of  $\lambda = 800$  nm, and  $\omega_0 = 351$  nm,  $z_e = 1650$  nm and  $V \approx 0.85$  fL for  $\lambda = 840$  nm. These values were validated in experiments with fluorescent latex microbeads for the  $xy$  resolution and with fluoresceine isothiocyanate (FITC) monolayers for the  $z$  resolution.<sup>[26]</sup> The detection unit is an avalanche photodiode (SPCM-AQ-131, EG&G Optoelectronics Canada) with a total detection efficiency of about 2% for C314 ( $\lambda_F = 480$  nm) and about 3% for C153 ( $\lambda_F = 532$  nm). The signal of the avalanche photodiode is directed to a multichannel scaler (MCD-2E, 7882, FAST ComTec) operated at 10 kHz (100  $\mu$ s/channel) or 100 kHz (10  $\mu$ s/channel) depending on the required resolution.

For the single-molecule experiments we used solutions (200 pmol L<sup>-1</sup>) of C153 and C314 (Radiant Dyes) in glycol p.a. (dynamic viscosity  $\eta = 16.1 \cdot 10^{-3}$  Pa·s). For measurements of TPE cross section and fluorescence lifetime 100 nmol L<sup>-1</sup> solutions of C153 and C314 were used.

## 4. Results and Discussion

### 4.1. Fluorescence Signals of C153 and C314

The TPE cross sections  $\delta$  and fluorescence lifetimes  $\tau_F$  of C153 and C314 were determined to completely characterise their fluorescence. The TPE cross section  $\delta$  of C153 in ethanol at  $\lambda = 800$  nm is  $47.4 \pm 0.8$  GM (1 GM =  $10^{-50}$  cm<sup>4</sup> s photon<sup>-2</sup>), and that of C314 in ethanol at  $\lambda = 840$  nm is  $16.4 \pm 0.5$  GM. Coumarin 1 was used as reference for measuring the relative TPE cross section.<sup>[27]</sup> The main error sources in these measurements were fluctuations of the laser power ( $\pm 0.1$  mW) and imprecisions due to dilution of the solutions ( $\pm 1$  nmol L<sup>-1</sup>) and determination of the total detection efficiency ( $\pm 0.1\%$ ). The resulting errors are similar to the deviations determined experimentally. The fluorescence lifetimes of C153 and C314 in glycol were determined with the same setup described before, except that the avalanche photodiode was replaced by an ICCD camera

(PicoStar, LaVision) with a gate width of 200 ps. The fluorescence lifetime  $\tau_f$  is  $3.1 \pm 0.1$  ns for C153 and to  $3.3 \pm 0.1$  ns for C314. These results agree with previously published fluorescence lifetimes of C153 and C314.<sup>[19,28]</sup>

With our kinetic rate model the optimal laser parameters, for example, pulse width, can be determined for any TPE setup and for any molecule with low ISC rate. In the following, we show the applicability of this model by comparing the simulated data with our experimental data.

In two-photon fluorescence microscopy we expect the fluorescence signal to scale quadratically with the excitation flux  $\phi$ . However, it is known that at high laser fluxes in the excitation volume this relation is no longer valid due to the increased influence of induced emission. The excitation flux at which the fluorescence signal reaches the maximum value is denoted as saturation flux. The excitation flux  $\phi_0$  during the pulse is directly proportional to the mean laser power  $\langle P \rangle$  over space and time at the sample [Eq. (22)].

$$\langle P \rangle = \phi_0 \frac{\tau_p}{\tau_0} \pi \omega_0^2 \quad (22)$$

Thus, under identical experimental conditions, that is, the same laser characteristics  $\tau_p$  and  $\tau_0$  and the same excitation volume, the dependence of the fluorescence signal on the flux  $\phi$  can be deduced from the dependence of the fluorescence signal on the mean power  $\langle P \rangle$ .

Experiments performed with  $100 \text{ nmol L}^{-1}$  solutions of C153 and C314 show that for mean excitation powers  $\langle P \rangle$  of less than 80 mW, the quadratic dependence of the total fluorescence signal  $F$  on the laser power is validated (the slope recovered from the double-logarithmic plot  $F(\langle P \rangle)$  is  $1.95 \pm 0.05$  for C153 and  $2.03 \pm 0.03$  for C314). Consequently, the saturation effect is negligible at powers of less than 80 mW (data not shown).

Employing our kinetic rate model, we simulated the dependence of the fluorescence signal  $F_S$  emitted by a single molecule during the period  $\tau_0$  on the mean laser power  $\langle P \rangle$  (Figure 2).

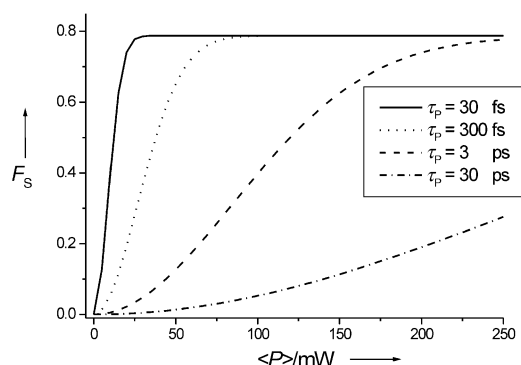


**Figure 2.** The fluorescence signal  $F_S$  emitted by a single C153 molecule during the period  $\tau_0 + \tau_p$  as a function of the mean laser power  $\langle P \rangle$  at the sample. Parameters employed in the kinetic rate model:  $\delta = 47.4 \text{ GM}$ ,  $\tau_f = 3.1 \text{ ns}$ ,  $\tau_0 = 13 \text{ ns}$ ,  $\omega_0 = 334 \text{ nm}$ ,  $\sigma = 1.7 \cdot 10^{-23} \text{ cm}^2$ . Considered pulse widths  $\tau_p = 30 \text{ fs}$ ,  $300 \text{ fs}$ ,  $3 \text{ ps}$ ,  $30 \text{ ps}$  (simulated data).

The fluorescence signal  $F_S$  integrated over the period  $\tau_0$  was calculated from Equation (13). The probability of occupancy  $S_1(\tau_p)$  is the solution of set of differential Equations (6), for which the initial conditions are those for  $i=1$ . In this case the long-term effects of diffusion and photobleaching are neglected, as is appropriate for measurements at high concentrations. The mathematical expression of  $F_S$  is given by Equation (23).

$$F_S = g_2(t'f_0(\tau_p, \tau_0, k_f)) \quad (23)$$

In this way, maximum-saturation mean laser powers at  $\delta F_S / \delta \langle P \rangle = 0$  of 134 mW for C153 and of 226 mW for C314 were obtained for a pulse width of 300 fs. A deviation from the linearity in the double-logarithmic plot  $\lg(F_S)$  versus  $\lg(\langle P \rangle)$  is already observed at about 50% of the maximum-saturation mean laser power. These results were verified by the experiment.

The dependence of the fluorescence signal  $F_S$  on  $\langle P \rangle$  deduced from the kinetic rate model is equivalent to the experimentally determined dependence of the total fluorescence signal  $F$  on  $\langle P \rangle$ , because both the signal  $F_S$  of the individual molecule and the total signal  $F$  stemming from a large group of molecules are not influenced by long-term effects of diffusion and individual photobleaching.

An important parameter which influences the dependence of the fluorescence signal  $F_S$  on the mean excitation power  $\langle P \rangle$  is the pulse width  $\tau_p$  [Eq. (23)]. As shown in Figure 2, the maximum-saturation level is reached at a lower mean laser power for a shorter pulse. Thus, we can conclude that ultrashort pulsed excitation is favourable in single-molecule experiments in which low mean laser powers at the sample are required, since the fluorescence signal already reaches the maximum value at such low powers. On the other hand, at mean powers  $\langle P \rangle$  above 50 mW a decrease in the pulse width from 300 to 30 fs or even less will not influence the fluorescence signal. Thus, any efforts to reduce the pulse width are unnecessary.

The count rate at the detector originating from the emission of an individual molecule at a mean laser power  $\langle P \rangle$  of 40 mW is on average 32 kHz for C153 and 29 kHz for C314. The background count rate of glycol, including a dark count rate of 200 Hz, amounts to 600 Hz under the same conditions. Thus, an average burst is detected with a signal-to-background ratio (SBR)<sup>[22]</sup> of about 53 for C153 and about 48 for C314 at  $\langle P \rangle = 40 \text{ mW}$ . The rather low mean SBR<sup>[23]</sup> is acceptable considering that neither C153 nor C314 was excited at its absorption maximum and the experiments are performed under nonsaturation conditions.

## 4.2. Autocorrelation Analysis

In this section we verify the applicability of the developed kinetic rate model to single-molecule FCS by approximating experimental fluorescence autocorrelation functions with the simulated function  $G_{\text{fit}}(\tau)$ .

The processes which in our case influence the time profile of the autocorrelation function  $G(\tau)$  of the fluorescence signal  $F(t)$  are photobleaching and diffusion. Photobleaching is quantified

by the photobleaching rate  $q_{pb}$ , which is  $\sigma\phi_0$  during the laser pulse and zero during the dark period between consecutive pulses. Since the cross section  $\sigma$  of the transition  $S_n \leftarrow S_1$  (photobleaching cross section) is a molecular constant, the only parameter which can lead to variations in the photobleaching rate during the laser pulse is the excitation flux  $\phi_0$ . Indirectly, photobleaching is also influenced by the pulse width  $\tau_p$  and by the laser repetition rate  $1/\tau_0$ . These aspects will not be discussed here.

Since for given pulse width  $\tau_p$  and repetition rate  $1/\tau_0$  the excitation flux  $\phi_0$  is proportional to the mean laser power  $\langle P \rangle$  at the sample, we can investigate the effect of photobleaching on the autocorrelation function by analysing the time profile of the autocorrelation functions at different mean laser powers  $\langle P \rangle$  (Figure 3). The time profile of the autocorrelation function is characterised by the amplitude  $A$  and by the decay time  $\tau_{\text{decay}}$ . The decay time  $\tau_{\text{decay}}$  is defined as the time until the autocorrelation function decreases to  $1/e$  of its initial value  $A$ . This period is roughly equivalent to the mean dwell time of the molecule in the volume  $V$ , which is affected by both photobleaching and diffusion.

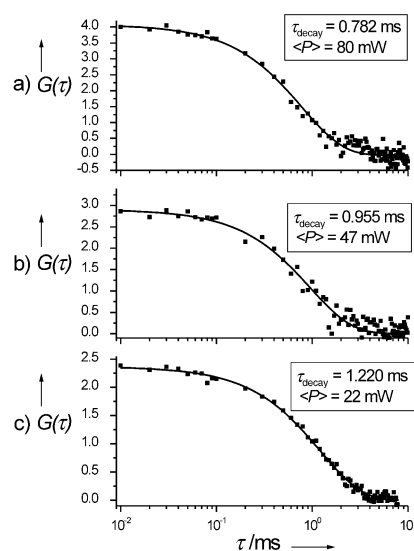


**Figure 3.** Autocorrelation functions of the fluorescence signal of single C153 molecules measured at a) 80 mW,  $\xi = 0.5$ , b) 47 mW,  $\xi = 0.48$  and c) 22 mW,  $\xi = 0.52$ . Parameters employed in the kinetic rate model:  $\delta = 47.4$  GM,  $\tau_F = 3.1$  ns,  $\tau_0 = 13$  ns,  $\tau_p = 300$  fs,  $\omega_0 = 334$  nm,  $\sigma = 1.7 \cdot 10^{-23}$  cm<sup>2</sup> and  $\tau_D = 1.25$  ms (experimental data fitted by the simulated function  $G_{\text{fit}}(\tau)$ ).

The decay time of the experimental autocorrelation curves of a 200 pmol L<sup>-1</sup> solution of C153 (Figure 3) measured at 22, 32, 40, 47, 55 and 80 mW decreases with increasing mean laser power  $\langle P \rangle$ , while under the same conditions the amplitude tends to increase. This indicates that photobleaching plays an important role in the power range 20–80 mW. However, neither the decay time nor the amplitude of the autocorrelation functions offers the possibility of a quantitative distinction between the effects of diffusion and photobleaching. Neverthe-

less, when the theoretical function  $G_{\text{fit}}(\tau)$  is fitted to the experimental autocorrelation curves, we can determine the photobleaching cross section ( $\sigma = 1.7 \cdot 10^{-23}$  cm<sup>2</sup> for C153) and the mean diffusion time ( $\tau_D = 1.25$  ms for C153). From the amplitude of the autocorrelation functions we also obtained the average number of molecules in the volume  $V$  ( $N = 0.115$ ). This value agrees with the value of  $N_C = 0.088$  calculated from the bulk concentration  $C$  of the solution as  $N_C = C \cdot V$ .

For  $N = 0.115$  it is implausible that more than one molecule resides at a time inside the excitation volume, since the probability  $P_2 = 5.6 \cdot 10^{-3}$  of finding two molecules in  $V$  as compared to the probability  $P_1 = 0.1$  of finding only one molecule in  $V$  is rather low. For calculating these probabilities, we assumed that random motion of the molecules through the excitation volume is governed by Poissonian statistics. In any case, we can be sure that basically only one molecule is detected at a time.

Using our kinetic rate model, we can determine the dependence of the decay time  $\tau_{\text{decay}}$  and of the amplitude  $A$  on the mean laser power  $\langle P \rangle$  (Figure 4). Thus, we can delimit the power range in which diffusion predominates from the region in which both diffusion and photobleaching contribute to the time profile of the autocorrelation function.

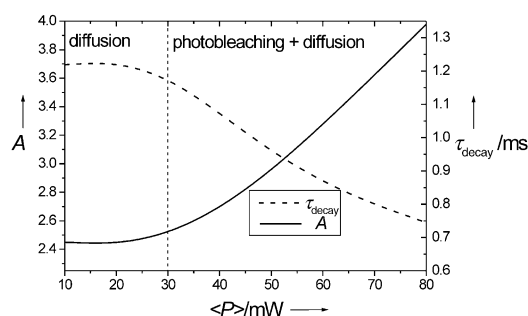


**Figure 4.** Dependence of the decay time  $\tau_{\text{decay}}$  and of the amplitude  $A$  of the autocorrelation function on the mean laser power  $\langle P \rangle$ . Employed parameters:  $\delta = 47.4$  GM,  $\tau_F = 3.1$  ns,  $\tau_0 = 13$  ns,  $\tau_p = 300$  fs,  $\omega_0 = 334$  nm,  $\sigma = 1.7 \cdot 10^{-23}$  cm<sup>2</sup>,  $N = 0.115$ ,  $\tau_D = 1.25$  ms,  $\xi = 0.5$  (results of the approximation of the experimental data by  $G_{\text{fit}}(\tau)$ ).

In the case of C153, the dependence of the decay time  $\tau_{\text{decay}}$  on the mean excitation power  $\langle P \rangle$  indicates that photobleaching plays an essential part in modelling the time profile of the autocorrelation function at laser powers  $\langle P \rangle$  higher than about 30 mW, but this effect vanishes for  $\langle P \rangle$  lower than 30 mW.

Experimentally it has been observed that photobleaching not only influences the time profile, but also the amplitude  $A$  of the autocorrelation function, that is, the amplitude of the autocorrelation function increases with increasing excitation power.<sup>[16]</sup> In our theoretical model, the amplitude  $A$  of the autocorrelation function  $G_{\text{fit}}(\tau)$  depends on  $N$  and  $\xi$  and additionally on the photobleaching parameters. Thus,  $N$  is the mean number of molecules present in the excitation volume and not just the mean number of fluorescing molecules and can be directly compared to  $N_C$ . The increase in the amplitude of the autocorrelation function with increasing mean excitation power

$\langle P \rangle$  in the range 30–80 mW (Figure 4) indicates once more that photobleaching plays a significant role in our experiment for  $\langle P \rangle$  higher than about 30 mW. For  $\langle P \rangle$  lower than 30 mW the amplitude of the autocorrelation function remains essentially constant, as expected.

The dependence of the decay time  $\tau_{\text{decay}}$  and the amplitude  $A$  of the fluorescence autocorrelation functions on the excitation power  $\langle P \rangle$  that results from our measurements is similar to well-known FCS results determined under the assumption of cw illumination.<sup>[9–17]</sup> In this way the correctness of our experiments and of the developed model is guaranteed. The main difference between our model and the well-known cw models, that is, the consideration of pulsed excitation, pulsed photobleaching and pulsed induced emission, is mirrored quantitatively in different photobleaching cross sections. With our model a photobleaching cross section  $\sigma$  of  $\approx 10^{-23}$  cm<sup>2</sup> was determined, while a cw model gave a value of  $\approx 10^{-17}$  cm<sup>2</sup> for the same parameter. Moreover, the good agreement between the experimental data of C153 and the simulated autocorrelation function  $G_{\text{fit}}(\tau)$  at different excitation powers indicates unequivocally that the photobleaching rate  $q_{\text{pb}}$  corresponding to the photobleaching pathway through  $S_n$  scales linearly with the excitation flux, and thus that the ground-state depletion rate scales cubically with the excitation flux. An approximation of the same experimental data with the autocorrelation function obtained from a kinetic rate model in which the photobleaching rate  $q_{\text{pb}}$  is considered to be independent of the excitation flux leads to discrepancies between simulation and the experiment.

Until now, we have primarily commented on the influence of photobleaching and only tangentially on the effect of diffusion on the autocorrelation function. The effect of diffusion on the fluorescence signal of individual molecules is analysed by studying the impact of the mean diffusion time  $\tau_D$  of a single C153 molecule through the volume  $V$  on the time profile of the autocorrelation function (Figure 5). As expected, the amplitude  $A$  of the autocorrelation function does not vary with mean diffusion time  $\tau_D$ , while the dwell time  $\tau_{\text{decay}}$  of a molecule in the excitation volume does. This behaviour is shown in Figure 6.

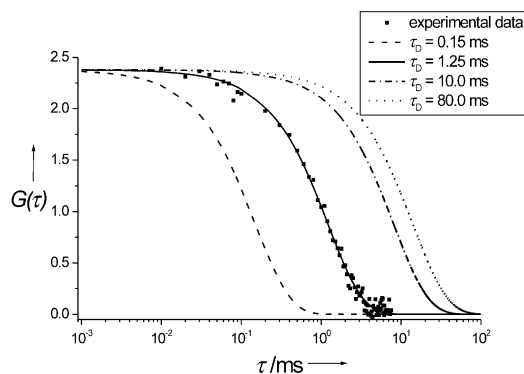


**Figure 5.** Simulated autocorrelation functions of C153 at different diffusion times. Employed parameters:  $\delta = 47.4$  GM,  $\tau_f = 3.1$  ns,  $\tau_D = 13$  ns,  $\tau_p = 300$  fs,  $\omega_0 = 334$  nm,  $\sigma = 1.7 \cdot 10^{-23}$  cm<sup>2</sup>,  $N = 0.119$ ,  $P = 22$  mW,  $\xi = 0.52$ .

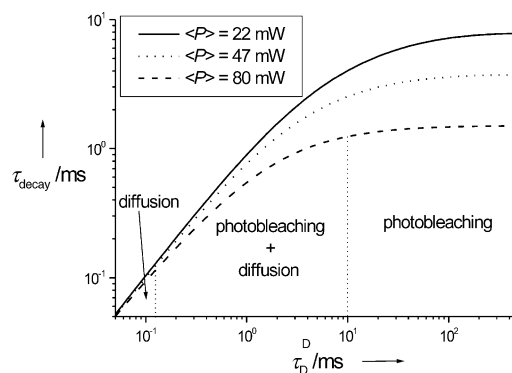


**Figure 6.** Dependence of the decay time  $\tau_{\text{decay}}$  (dwell time of a C153 molecule in the volume  $V$ ) on the mean diffusion time  $\tau_D$  at different mean excitation powers. The dwell time at large  $\tau_D$  (photobleaching time) depends on the excitation power and is 7.806 ms at  $\langle P \rangle = 22$  mW, 3.733 ms at  $\langle P \rangle = 47$  mW and 1.495 ms at  $\langle P \rangle = 80$  mW (simulated data).

For short diffusion times, the dwell time  $\tau_{\text{decay}}$  exhibits a linear dependence on  $\tau_D$ , that is,  $\tau_{\text{decay}}$  basically represents the diffusion time. With increasing diffusion time this dependence deviates from linearity, and for large diffusion times (at  $\langle P \rangle = 80$  mW, ca. 10 ms), the decay time barely varies with  $\tau_D$ . The dwell time  $\tau_{\text{decay}}$  in this range roughly corresponds to the photobleaching time. Thus, at each excitation power  $\langle P \rangle$ , we are able to delimit the  $\tau_D$  ranges in which only diffusion, only photobleaching or both processes influence the time profile of the autocorrelation function, as shown for  $\langle P \rangle = 80$  mW in Figure 6. Moreover, for diffusion times of about 1 ms and at excitation powers up to 80 mW, as in our experiment, photobleaching will not be predominant. This will only occur at higher laser powers or at longer diffusion times.

Note that the diffusion time  $\tau_D$  and the mean laser power  $\langle P \rangle$  are two independent parameters, and consequently Figures 4 and 6 represent two different effects on the autocorrelation function.

The influence of diffusion, that is, diffusion time  $\tau_D$ , on the fluorescence autocorrelation functions, that is, on the decay time  $\tau_{\text{decay}}$  and on the amplitude  $A$ , as shown in Figures 5 and 6, agrees with FCS experiments and FCS simulations performed by means of cw models.<sup>[9–17,22]</sup> This is a further verification of the correctness of our pulsed-illumination model.

By approximating the experimental autocorrelation curves of the fluorescence signal of a 200 pmol L<sup>-1</sup> solution of C314 with the simulated function  $G_{\text{fit}}(\tau)$ , we determined  $N = 0.119$ ,  $\sigma = 5 \cdot 10^{-23}$  cm<sup>2</sup> and  $\tau_D = 1.39$  ms ( $\xi \approx 0.5$ ). Also, in this case  $N = 0.119$  agrees with  $N_c = 0.102$ .

The photostability is an important factor in choosing appropriate dyes for single-molecule detection and spectroscopy. The photobleaching yield  $\varphi_{\text{pb}}$  and the ground-state depletion rate  $q_0$  are usually employed as indicators for the photostability of substances investigated by single-molecule FCS. However, in the case of two-photon excitation the main disadvantage of these indicators is their dependence on the excitation intensity and on the type of illumination, and thus they are usually specific for each experiment.

**Table 1.** Summary of the determined molecular parameters of C153 and C314:  $\sigma$  = photobleaching constant,  $\delta$  = two-photon absorption cross section,  $\tau_f$  = fluorescence lifetime,  $\tau_D$  = mean diffusion time and  $D$  = diffusion coefficient. The fluorescence lifetime of C153 was measured in ethanol.<sup>[19]</sup> For C153 in DMF an absorption cross section of  $\delta = 47 \pm 2$  GM at 800 nm is given in ref. [24] The deviation between the local diffusion coefficient  $D$  determined from the time profile of the autocorrelation function and the diffusion coefficient  $D^*$  calculated by using the Stokes–Einstein relation is acceptable, since the requirement of the Stokes–Einstein relation for molecules to be spherical is not sufficiently fulfilled by the studied coumarins. To our knowledge the photobleaching cross sections  $\sigma$  of C153 and C314 at 800 and 840 nm were not known up to now.

	$\sigma$ [cm <sup>2</sup> ]	$\delta$ [GM]	$\tau_f$ [ns]	$\tau_f^{\text{lit}}$ [ns]	$\tau_D$ [ms]	$D$ [cm <sup>2</sup> s <sup>-1</sup> ]	$D^*$ [cm <sup>2</sup> s <sup>-1</sup> ]
C153	$1.7 \times 10^{-23}$ (at 800 nm)	$47.4 \pm 0.8$ (at 800 nm)	$3.1 \pm 0.1$	3.4	1.25	$1.66 \times 10^{-6}$	$1.36 \times 10^{-6}$
C314	$5 \times 10^{-23}$ (at 840 nm)	$16.4 \pm 0.5$ (at 840 nm)	$3.3 \pm 0.1$	$3.316 \pm 0.196$	1.39	$1.64 \times 10^{-6}$	$1.36 \times 10^{-6}$

The photobleaching yield  $\varphi_{\text{pb}}^3$  is  $2 \times 10^{-3}$  for C153 and  $2.2 \cdot 10^{-3}$  for C314 at  $\langle P \rangle = 22$  mW.

The ground-state depletion rate  $q_0^4$  is  $0.213 \text{ ms}^{-1}$  for C153 and  $0.285 \text{ ms}^{-1}$  for C314 at  $\langle P \rangle = 80$  mW and is significantly lower than the ground state depletion rate determined for tetramethyl rhodamine (TMR)  $q_0 = 49 \text{ ms}^{-1}$  at saturation.<sup>[16]</sup>

Note that the photobleaching rate of TMR was determined by using a theoretical approach assuming two-photon cw excitation for the simulation of the autocorrelation functions.

## 5. Conclusion

We have presented a theoretical approach for the simulation of the autocorrelation functions acquired in two-photon excitation single-molecule FCS experiments. The main novel feature of this model is the consideration of pulsed illumination and its effect on the photobleaching rate, excitation rate and rate of induced emission.

Moreover, this theoretical approach opens the possibility to rigorously investigate the effect of laser characteristics such as pulse width and repetition rate on the fluorescence autocorrelation function. The main simplification is the assumption of rectangular profiles with respect to the laser flux, both spatially and temporally. It is easy to extend the model for any laser pulse profile and also for dyes with considerable ISC rates. However, in this case a simple analytical solution is not possible. Moreover, according to our results such an extension of the theoretical model is also unnecessary.

<sup>3</sup> The photobleaching yield is defined by Equation (h).

$$\varphi_{\text{pb}} = \frac{\text{no. of photobleached molecules}}{\text{total no. of laser pulses}} = \frac{\sigma \phi_0 \sum_{i=0}^{\tau_{\text{decay}}/\tau_0} S_{1p}^i(\tau_p, \phi_0)}{\tau_{\text{decay}}/\tau_0} \quad (\text{h})$$

We considered that only one molecule dwells in the excitation volume at a time, and thus only one molecule can be excited once during a laser pulse.

<sup>4</sup> The ground-state depletion rate is defined as Equation (i)

$$q_0 = \frac{1}{\tau_p} \int_0^{\tau_p} \frac{dS_1(t')}{dt'} dt' = \frac{1}{\tau_p} \int_0^{\tau_p} \sigma \phi_0 S_{1p}^1(t') dt' \quad (\text{i})$$

where  $S_{1p}^1$  is the probability of occupancy of the first singlet state during the first pulse  $i=1$  and was determined by solving set (6) of differential equations [Eq. (j)].

$$S_{1p}^1(t') = g_2(t') \quad (\text{j})$$

The initial conditions for set of Equations (6) in this case are  $a^1 = 1$  and  $b^1 = 0$ .

To prove the accuracy of our model we approximated experimental results with the simulated autocorrelation functions. The good agreement between the parameters determined from the autocorrelation function and those determined by other means validates the model.

Furthermore, we determined the molecular specific photobleaching cross section  $\sigma$  for both C153 and C314, which indicate photostability of these dyes independent of the experimental conditions. A comparison of the ground-state depletion rates of the studied dyes with that of TMR indicates that C153 and C314 are very suitable for single-molecule FCS due to their increased photostability under two-photon excitation. The essential experimental results are summarised in Table 1.

## Acknowledgements

This research was supported by the Bundesministerium für Bildung und Forschung (BMBF) under grant 13N7927.

**Keywords:** fluorescence · laser spectroscopy · photobleaching · photodynamic rate model · single-molecule studies

- [1] W. P. Ambrose, P. M. Goodwin, J. H. Jett, A. Van Orden, J. H. Werner, R. A. Keller, *Chem. Rev.* **1999**, *99*, 2929–2956.
- [2] S. Nie, R. N. Zare, *Annu. Rev. Biophys. Biomol. Struct.* **1997**, *26*, 567–596.
- [3] A. A. Deniz, T. Laurence, M. Dahan, D. S. Chelma, P. G. Schultz, S. Weiss, *Annu. Rev. Phys. Chem.* **2001**, *52*, 233–253.
- [4] W. E. Moerner, M. Orrit, *Science* **1999**, *283*, 1670–1676.
- [5] a) H. Qian, E. S. Elson in *Fluorescence Correlation Spectroscopy—Theory and Applications* (Eds: R. Rigler, E. S. Elson), Springer, Berlin, **2000**, pp. 65–82; b) W. W. Webb in *Fluorescence Correlation Spectroscopy—Theory and Applications* (Eds: R. Rigler, E. S. Elson), Springer, Berlin, **2000**, pp. 305–328.
- [6] S. R. Aragon, R. Pecora, *J. Chem. Phys.* **1976**, *64*, 1791–1803.
- [7] T. Wohland, R. Rigler, H. Vogel, *Biophys. J.* **2001**, *80*, 2987–2999.
- [8] a) R. Rigler, L. Edman, Z. Földes-Papp, S. Wennmalm in *Single molecule Spectroscopy, Nobel Conference Lectures* (Eds: R. Rigler, M. Orrit, T. Basché), Springer, Berlin, **2001**, pp. 177–195; b) T. Wohland, K. Friedrich-Bénet, H. Pick, A. Preuss, R. Hovius, H. Vogel in *Single molecule Spectroscopy, Nobel Conference Lectures* (Eds: R. Rigler, M. Orrit, T. Basché), Springer, Berlin, **2001**, pp. 195–211.
- [9] J. Widengren, U. Mets, R. Rigler, *J. Phys. Chem.* **1995**, *99*, 13368–13379.
- [10] J. Widengren, J. Dapprich, R. Rigler, *Chem. Phys.* **1996**, *216*, 417–426.
- [11] J. Widengren, R. Rigler, *Bioimaging* **1996**, *4*, 149–157.
- [12] A. Molski, J. Hofkens, T. Gensch, N. Boens, F. C. De Schryver, *Chem. Phys. Lett.* **2000**, *318*, 325–332.
- [13] A. Molski, *J. Chem. Phys.* **2001**, *114*, 1142–1147.
- [14] C. Egeling, J. Widengren, R. Rigler, C. A. M. Seidel, *Anal. Chem.* **1998**, *70*, 2651–2659.

- [15] P. Schwille, U. Haupts, S. Maiti, W. W. Webb, *Biophys. J.* **1999**, *77*, 2251–2265.
- [16] P. S. Dittrich, P. Schwille, *Appl. Phys. B* **2001**, *73*, 829–837.
- [17] J. Mertz, *Eur. Phys. J. D* **1998**, *3*, 53–66.
- [18] K. I. Priyadarsini, D. B. Naik, P. N. Moorthy, *J. Photochem. Photobiol. A* **1989**, *46*, 239–246.
- [19] G. Jones II, W. R. Jackson, C. Choi, *J. Phys. Chem.* **1985**, *89*, 295.
- [20] The intersystem crossing rate  $k_{ISC}$  increases with decreasing energy gap  $\Delta E$  between  $S_1$  and  $T_1$ .  $\Delta E$  between  $S_1$  and  $T_1$  is for rhodamines 0.14 eV,<sup>[14]</sup> and for C153 0.86 eV.<sup>[18]</sup>  $k_{ISC}$  is for rhodamines about  $10^6 \text{ s}^{-1}$ , and for the studied coumarins about  $10^2 \text{ s}^{-1}$ . The high rigidity of the C153 and C314 molecules also contributes to their low ISC rates.<sup>[18]</sup> See M. S. A. Abdel-Mottaleb, M. S. Antonious, M. M. Abo-Aly, L. F. M. Ismaiel, B. A. El-Sayed, A. M. K. Sherief, *J. Photochem. Photobiol. A* **1989**, *50*, 259–273.
- [21] G. H. Patterson, D. W. Piston, *Biophys. J.* **2000**, *78*, 2159–2162.
- [22] J. Mertz, C. Xu, W. W. Webb, *Opt. Lett.* **1995**, *20*, 2532–2534.
- [23] L. Brand, C. Eggeling, C. Zander, K. H. Drexhage, C. A. M. Seidel, *J. Phys. Chem. A* **1997**, *101*, 4313–4321.
- [24] G. D. Reid, K. Wynne in *Encyclopedia of Analytical Chemistry* (Ed: R. A. Meyers), Wiley, Chichester, **2000**, pp. 13 644–13 670.
- [25] R. Wolleschensky, T. Feurer, R. Sauerbrey, U. Simon, *Appl. Phys. B* **1997**, *67*, 87–94.
- [26] A. Schönle, M. Glatz, S. W. Hell, *Appl. Opt.* **2000**, *39*, 6306–6311.
- [27] A. Fischer, C. Cremer, H. Z. Stelzer, *Appl. Opt.* **1995**, *34*, 1989–2003.
- [28] D. S. Elson, J. Siegel, S. E. D. Webb, S. Lévêque-Fort, M. J. Lever, P. M. W. French, K. Lauritsen, M. Wahl, R. Erdmann, *Opt. Lett.* **2002**, *27*, 1409–1411.

---

Received: June 18, 2003 [F 881]

Revised: December 16, 2003